Optics Communications 578 (2025) 131515

Contents lists available at ScienceDirect

Optics Communications

journal homepage: www.elsevier.com/locate/optcom

Dipole-like scattering by Rayleigh-sized particles with medium-matched real and general imaginary part of the refractive index

Sami Labidi [a], Justin B. Maughan [b,a], Kurt Ehlers [c], Prakash Gautam [d], Christopher M. Sorensen [a], Hans Moosmüller [d,*]

[a] Department of Physics, Kansas State University, 116 Cardwell Hall, 66506-2601, Manhattan, KS, USA
[b] Pratt Community College, 348 NE SR 61, 67124, Pratt, KS, USA
[c] Mathematics Department, Truckee Meadows Community College, 7000 Dandini Blvd., 89512, Reno, NV, USA
[d] Laboratory for Aerosol Science, Spectroscopy, and Optics, Desert Research Institute, 2215 Raggio Parkway, 89512, Reno, NV, USA

ARTICLE INFO

Keywords:
Particle scattering
Complex refractive index
Medium-matched real part of the refractive index
Rayleigh scattering
Perfect conductor scattering
Electric and magnetic dipole scattering

ABSTRACT

We explore Mie scattering by a homogeneous, spherical particle of radius much smaller than the wavelength of light and a complex refractive index. When the medium refractive index is a real number equal to the real part of the particle refractive index, the effective particle refractive index is of the form $1 + i\kappa$. In this case, scattering is caused solely by the imaginary part κ of the particle refractive index, resembling Rayleigh scattering at small values and perfect conductor scattering at large values of κ. We employ a Mie computer program to simulate the scattering in this case; we plot the results and see that as κ increases, the scattering of s-polarized light becomes more anisotropic, the backscattering intensity brightens while the forward scattering intensity dims. To explain our results theoretically, we explore how the Mie equations reduce for constraints of size parameter $x \ll 1$ and a refractive index of the form $m = 1 + i\kappa$, though our analysis holds for arbitrary m so long as $Re(mx) \ll 1$. We find that such small particles may be described by a dipole with appropriate electric and magnetic dipole moments. Simple equations are given describing the scattering by these particles. Finally, we supplement our results with diagrams visualizing why we see the pattern found.

1. Introduction

We consider the scattering of light of wavelength λ by small spherical particles of radius R immersed in a refractive, non-absorbing medium. These particles have a size parameter of $x \equiv kR \ll 1$, where $k = 2\pi/\lambda$ is the wavenumber of incident light. Scattering by such a particle obeys the Rayleigh formula if $|mx| \ll 1$, where $m = n + i\kappa$ is the complex refractive index of the particle [1,2]. If $x \ll 1$, but the condition $|mx| \ll 1$ may not be met, we use the expression "electric dipole terms of the Mie expansion (ED)" instead of "Rayleigh". If such a particle is submerged in a medium of purely real refractive index also equal to n, then its scattering is identical to the scattering by a particle of relative refractive index $m_{rel} = \frac{n+i\kappa}{n} = 1 + \frac{i\kappa}{n} = 1 + i\kappa_{rel}$ in vacuum [3,4]. Therefore, we consider scattering by small spherical particles with refractive index of the form $m = 1 + i\kappa$ (dropping the subscript "rel"), for values of κ over several orders of magnitude. The real part of the refractive index is "inconsequential" in this case, so κ alone is responsible for the scattering by such a particle. Note that if $\kappa = 0$, $m = 1$, and there is no particle scattering because the particle is optically identical to the surrounding medium. The case of $n = 1$, with scattering solely caused by κ, contrasts with the most commonly considered case of $\kappa = 0$, where scattering is solely caused by n. In addition to intellectual curiosity, this study also has practical applications including (1) the remote sensing of phytoplankton suspended in water where $n \approx 1$ with high values of κ [5] (however only picoplankton approaches the Rayleigh regime) and (2) using colloids of nano particles for the determination of particle complex refractive indices [6,7].

Previous work has shown that the parameter $\kappa kR = \kappa x$, the inverse of the relative optical penetration depth, is a universal parameter for the optics of absorbing particles in many situations [2,8]; that light reflected off the surface of particles becomes dominant for both scattering and absorption at $\kappa \gtrsim 2$ [9]; and that perfectly conducting particles of size parameter $x \ll 1$ scatter light according to a single-dipole approximation (herein abbreviated SDA) [10].

The ED and SDA formulae are both limiting-case approximations to

* Corresponding author.
E-mail addresses: slabi@mit.edu (S. Labidi), justinm@prattcc.edu (J.B. Maughan), kehlers@tmcc.edu (K. Ehlers), Prakash.Gautam@dri.edu (P. Gautam), sor@phys.ksu.edu (C.M. Sorensen), Hans.Moosmuller@dri.edu (H. Moosmüller).

https://doi.org/10.1016/j.optcom.2025.131515
Received 18 October 2024; Received in revised form 7 January 2025; Accepted 12 January 2025
Available online 13 January 2025

the much more complicated Mie theory of light scattering. In this paper, these approximations will be tested against exact solutions determined by the Mie equations. Using a Mie computer program, we “empirically” explore how the scattering by $x \ll 1$ particles of refractive index $1+ i\kappa$ evolves from the ED regime to the SDA regime. Once this empirical background is established, we provide a theoretical explanation involving the superposition of an electric and a magnetic dipole. We provide equations that (1) describe scattering by $x \ll 1$ particles of refractive index $m = 1 + i\kappa$ for general κ and (2) are consistent with our Mie results.

2. Theory

First, we state equations relevant to our discussion. We assume the magnetic permeability of the particle equals the magnetic permeability of the medium. The differential cross section of light scattered by a particle obeying $|mx| \ll 1$ with linearly polarized light incident is given by the ED formulae that are based on the Lorentz-Lorenz factor $LL(m) = (m^2-1)/(m^2+2)$ [11,12], which we simplify by setting $n = 1$ and consequently $m = 1 + i\kappa$ [13,14] as

$$\frac{dC_{s,ED}}{d\Omega} = k^4R^6\left|\frac{m^2-1}{m^2+2}\right|^2 = k^4R^6\frac{\kappa^4+4\kappa^2}{(3-\kappa^2)^2+4\,\kappa^2} \tag{1a}$$

$$\frac{dC_{p,ED}}{d\Omega} = k^4R^6\left|\frac{m^2-1}{m^2+2}\right|^2\cos^2\theta = k^4R^6\frac{\kappa^4+4\kappa^2}{(3-\kappa^2)^2+4\,\kappa^2}\cos^2\theta. \tag{1b}$$

The subscript “s” stands for the s (perpendicular) polarization, and “p” stands for the p (parallel) polarization. Simplified by setting $m = 1 + i\kappa$, for unpolarized light the total scattering cross section $C_{sca,ED}$ is the average of s- and p-cross sections integrated over all scattering directions (i.e., $\Omega = 4\pi$) and can be written as

$$C_{sca,ED} = \frac{8\pi k^4R^6}{3}\left|\frac{m^2-1}{m^2+2}\right|^2 = \frac{8\pi k^4R^6}{3}\frac{\kappa^4+4\kappa^2}{(3-\kappa^2)^2+4\,\kappa^2}. \tag{2}$$

According to Jackson [10], for a *perfectly conducting* sphere of size parameter $x \ll 1$, the differential cross section of linearly polarized light, as derived using a single-dipole approximation (SDA) and the boundary conditions for a perfect conductor [10], can be written as

$$\frac{dC_{s,SDA}}{d\Omega} = k^4R^6\left(1-\frac{1}{2}\cos\theta\right)^2 \tag{3a}$$

$$\frac{dC_{p,SDA}}{d\Omega} = k^4R^6\left(\frac{1}{2}-\cos\theta\right)^2, \tag{3b}$$

where θ is the scattering angle, the angle between the wavevector of incident light and the vector pointing from the center of the sphere to the observer. Jackson’s formulae originally included a factor of one half, but we removed it since he assumed unpolarized incident light. This SDA formulation approximates the sphere as an electric *and a* magnetic dipole, whereas the ED formulation assumes a negligible magnetic dipole moment. Integrating the average of the s- and p-cross sections in Eq. (3) over all scattering directions (i.e., $\Omega = 4\pi$) yields the total scattering cross section as

$$C_{sca,SDA} = \frac{10\pi k^4R^6}{3}. \tag{4}$$

A similarity between ED and SDA scattering is that both scale with the quantity k^4R^6. A notable distinction between ED and SDA scattering is that while ED scattering for s polarization is isotropic, SDA scattering exhibits strong angular dependence. From Eq. (3) the ratio of scattering intensities in the forward direction to the backward direction of SDA scattering is $I(0^\circ)/I(180^\circ) = 1/9$, independent of polarization. Moreover, the total cross section of SDA scattering is higher by a factor of 1.25 than that of ED scattering in the (fictional) limit $\kappa \to \infty$, which could be interpreted as the magnetic dipole contributing one quarter of the total scattering cross section contribution of the electric dipole.

Additionally, note that $|mx|$ becomes $|(1+i\kappa)x| \approx \kappa x$ when $\kappa \gg 1$. Since large κ may be used to model conductors, a perfect conductor with $\kappa \to \infty$ clearly breaks the $|mx| \approx \kappa x \ll 1$ constraint of Rayleigh scattering. It is assuring that these two wildly different equations do not model overlapping regimes but still yield similar results for the total scattering cross section.

Also of consideration is the asymmetry parameter, denoted by g. The asymmetry parameter is a dimensionless number between -1 and 1 that describes how much more light is scattering in the forward hemisphere compared to the backward hemisphere [1]. An asymmetry parameter of 0 means an equal amount of light is scattered into both directions. Quantitatively, the asymmetry parameter g is defined as

$$g = \frac{1}{2}\int_0^\pi P(\theta)\sin\theta\cos\theta d\theta, \tag{5}$$

where $P(\theta) = \frac{4\pi}{C_{sca}}\frac{dC}{d\Omega}$ is the phase function. Since ED scattering is symmetric about $\theta = 90^\circ$, it has an asymmetry parameter of 0 in the limit of $x \to 0$ [1]. Using Eqs. (3) and (5), one can show that SDA scattering has an asymmetry parameter of $-2/5 = -0.4$, indicating enhanced backscattering.

3. Results

We only consider the s (perpendicular) polarization for now. In Figure (1), the differential scattering cross section of s-polarized light, as calculated via the Mie equations, normalized to the scale factor k^4R^6, is plotted versus scattering angle for multiple values of κx. The size parameter x was held constant for a wavelength of 532 nm. The SDA and ED formulae, taken to the limit $\kappa \to \infty$, are also shown.

From Fig. (1a), we observe that small particles (i.e., $R = 10$ nm) such that $m = 1 + i\kappa$ and $|mx| < 1$ scatter light isotropically, consistent with the ED formulation. Small particles with $|mx| > 1$, due to large values of κ, however, scatter light anisotropically and have negative asymmetry parameters. As we will demonstrate later, the asymmetry parameter decreases to -0.4 as κ approaches infinity. Finally, we see that in the limit of $\kappa \to \infty$, scattering by small particles matches the SDA. By contrast, the ED formulation does not approach the SDA formulation when κ is taken to infinity.

Fig. (1b) is a plot nearly identical to Fig. (1a) but for a larger particle radius of $R = 30$ nm. We see that as for the 10 nm particle radius, small particles with $|mx| < 1$ scatter light roughly isotropically. For the larger radius of 30 nm, however, there is a very slight enhancement in the forward direction. The 30 nm particle with $|mx| \approx 1$ does not have this enhancement in the forward direction. Also, this 30 nm particle with $|mx| \approx \kappa x = 1$ scatters more total light than for any other value of κx shown. Finally, we observe that 30 nm particles with $|mx| \gg 1$ scatter light anisotropically, approaching the SDA formula in the limit $\kappa \to \infty$.

In Fig. (2a), s-polarized differential cross section in the forward direction ($\theta = 0^\circ$) is plotted versus κ on a log-log plot. Note that this time, the differential cross section was not normalized to the scale factor k^4R^6; this was done to ensure that the lines for different particle radii stay separate. We observe that small particles with $m = 1 + i\kappa$ scatter light in the forward direction with intensity proportional to κ^2 when $\kappa \ll 1$. This is consistent with Eq. (1) when $\kappa \ll 1$. For both sizes shown, the forward scattering reaches a maximum at $\kappa \approx 2$. This is consistent with Fig. (1b), where the line for $\kappa \approx 2.9$ indicates more scattering than for any other value of κ shown. We also notice that the 30 nm particle achieves $|mx| = 1$ at a smaller κ than the 10 nm particle; congruently, the Mie curve for the 30 nm particle departs from its ED curve at a smaller κ than for the 10 nm particle. As $\kappa \to \infty, I(0^\circ)$ for the 10 nm particle was 3.9 times smaller for the Mie curve than the ED curve. This roughly agrees with SDA scattering, whose $I(0^\circ)$ is exactly 4 times smaller than the value of

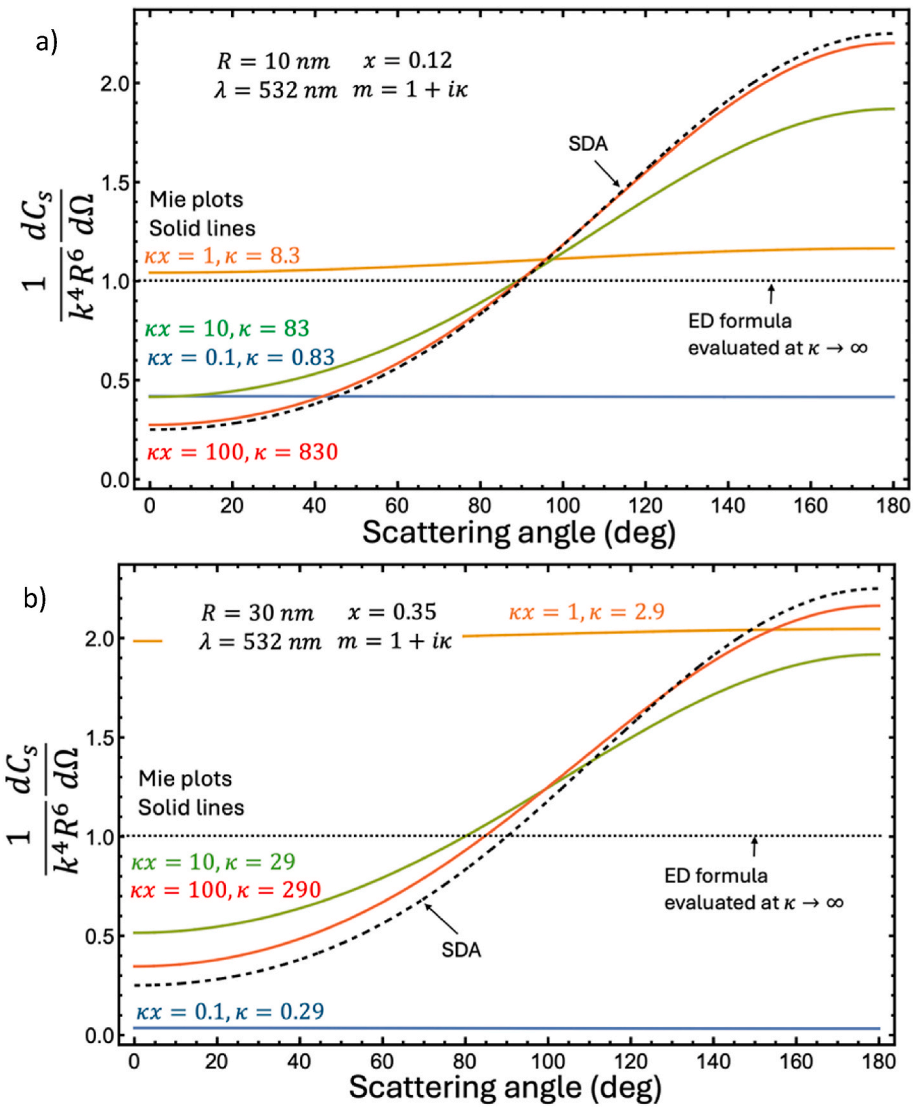

Fig. 1. | Differential scattering cross section of s-polarized light versus scattering angle for a spherical particle of radius (a) 10 *nm* and (b) 30 *nm* and incident light wavelength 532 *nm*. The colored, solid lines were calculated using the Mie equations. The dashed line was calculated using SDA equations (i.e., Eq. (3)); the dotted line was calculated using ED equations (i.e., Eq. (1)).

$I(0^{\circ})$ of ED scattering. As $\kappa \to \infty, I(0^{\circ})$ for the 30 nm particle was 3.1 times weaker for the Mie curve than the ED curve. This doesn't perfectly agree with SDA scattering, but note that the size parameter $x = 0.35$ of this particle is a bit high for the comfort of the SDA, which is valid for $x \ll 1$.

Fig. (2b) is very similar to Fig. (2a) except that it shows scattered light intensity in the backward direction ($\theta = 180^{\circ}$). As in the forward direction, we observe that small particles with $m = 1 + i\kappa$ scatter light in the backward direction with intensity proportional to κ^2 when $\kappa \ll 1$, consistent with Eq. (1). This suggests isotropic scattering when $\kappa \ll 1$. For both sizes shown, the backward scattering reached a maximum at $\kappa \approx 2$, which we confirmed by taking the first derivative of the identical κ dependance in Eqs. (1a), (1b) and (2) and setting it to zero, thereby, confirming the observation in Fig. 2 with the one physical solution of $\kappa = 2.091$.

We also notice that the 30 nm particle achieved $|mx| = 1$ at a smaller κ than the 10 nm particle; congruently, the Mie curve of the 30 nm particle departed from its ED curve at a smaller κ than for the 10 nm particle. As $\kappa \to \infty, I(180^{\circ})$ for the 10 nm particle was 2.24 times stronger for the Mie curve than the ED curve. This agrees with SDA scattering since $\frac{I_{SDA}(180^{\circ})}{I_{Ray}(180^{\circ})} = \frac{9}{4} = 2.25$. As $\kappa \to \infty, I(180^{\circ})$ for the 30 nm particle was 2.19 times stronger for the Mie curve than the ED curve. This roughly agrees with SDA scattering. Note that in contrast with forward scattering, Mie backscattering is stronger than ED backscattering for large κ. In fact, $I(180^{\circ})$ for Mie is larger in the limit $\kappa \to \infty$ than the value of $I(180^{\circ})$ for Mie or ED at the local maximum $\kappa_{maxsca} \approx 2$. This is consistent with Fig. (1b), where the curve with $\kappa \approx 2.9$ depicts slightly less scattered light at 180° than the curves with large κ.

From Fig. (2) we qualitatively see that the $|mx| \ll 1$ constraint on Rayleigh scattering holds up very well. In fact, for these small $m = 1 + i\kappa$ particles, Mie and Rayleigh theory agree reasonably well until $|mx| \gtrsim 1$. Zero and 180° are, however, the most extreme angles, and we saw in Fig. (1) that Mie and Rayleigh scattering at these angles depart from each other before they do so at the other angles. Of interest is a more quantitative determination of the point at which ED scattering as a whole fails to describe scattering by $x \ll 1$ particles with refractive index $m = 1 + i\kappa$, and how scattering from these particles transitions into SDA scattering.

In Fig. (3), the asymmetry parameter of Mie scattering is plotted versus κx for particles of various sizes much smaller than the wavelength of incident light. First, note that only the green curve can be seen—meaning all curves collapsed on top of each other. This suggests that for $m = 1 + i\kappa$ and particles much smaller than the wavelength of

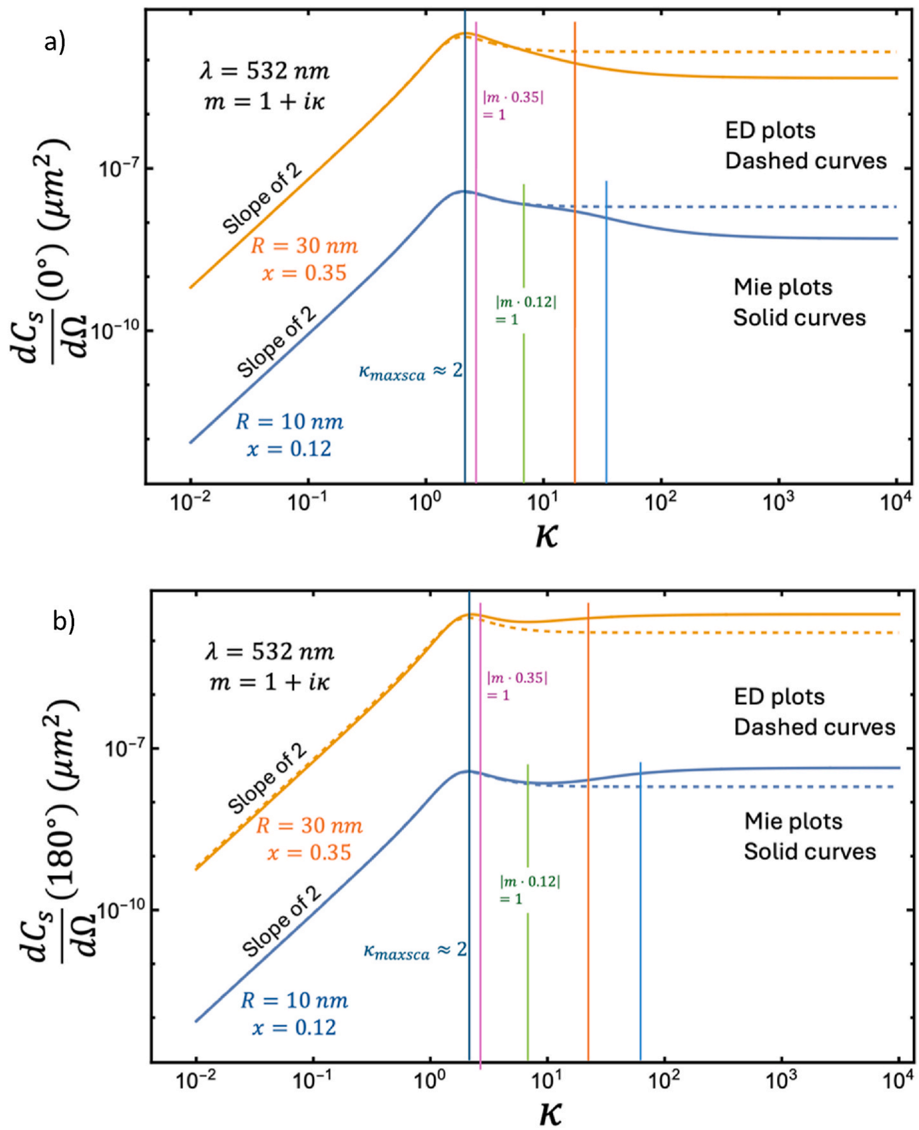

Fig. 2. | Log-log plot of s-polarized differential cross section in the (a) forward direction and (b) backward direction versus κ. The blue curves use a particle radius of 10 *nm*, and the orange curves use a particle radius of 30 *nm*. The dark blue vertical line depicts the κ with the maximum cross section. The green and purple vertical lines show where $|mx| = 1$ for the 10 *nm* and 30 *nm* particles, respectively. The blue and orange vertical lines show where the Mie curve significantly disagrees with the ED curve for the 10 *nm* and 30 *nm* particles, respectively.

incident light, the asymmetry parameter g is a function of a single variable, κx. For small values of κx, the asymmetry parameter was near-zero, as predicted by Rayleigh scattering. By the time $\kappa x \approx 1$, the asymmetry parameter has departed from zero, becoming negative. This can be seen in a different perspective in Fig. (1a), where the $\kappa x = 1$ curve has slightly higher backscattering than forward scattering. For $\kappa x \approx 4$, the asymmetry parameter is unmistakably negative, taking the value of -0.2, halfway between its minimum of -0.4 and its maximum of 0. As $\kappa x \rightarrow \infty$, the asymmetry parameter approaches -0.4, in agreement with SDA scattering.

4. Differential scattering cross section for a particle with small Re(mx)

In this section, we derive simple expressions using the electric and magnetic dipole terms of the Mie solution for the differential scattering cross sections of a small sphere for which $Re(mx) \ll 1$ as functions of the scale factor k^4R^6, refractive index m, scattering angle θ, and inverse relative optical penetration depth κx. For small κx these give the ED scattering cross sections (Eqs. (1) and (2)) and for large κx we recover the SDA approximation (Eqs. (3) and (4)).

The differential scattering cross sections of a sphere for s and p polarized light are given by [2].

$$\frac{dC_s}{d\Omega} = \frac{1}{k^2}\left|\sum_n \frac{2n+1}{n(n+1)}(a_n\pi_n(\cos\theta) + b_n\tau_n(\cos\theta))\right|^2 \tag{6a}$$

$$\frac{dC_P}{d\Omega} = \frac{1}{k^2}\left|\sum_n \frac{2n+1}{n(n+1)}(a_n\tau_n(\cos\theta) + b_n\pi_n(\cos\theta))\right|^2, \tag{6b}$$

where a_n and b_n are functions of m and x and can interpreted as the coefficients of a multipole expansion, with the a_n terms correspond to electric multipole terms, and the b_n terms correspond to magnetic multipole terms. π_n and τ_n are single-variable functions used to characterize the angular dependence of the scattering.

Below, we find approximate forms for the first few normal modes by using the equations for a_n and b_n given by Bohren and Huffman [13]; also, note that since $x \ll 1$, we may approximate terms of the form $f(x)$ by

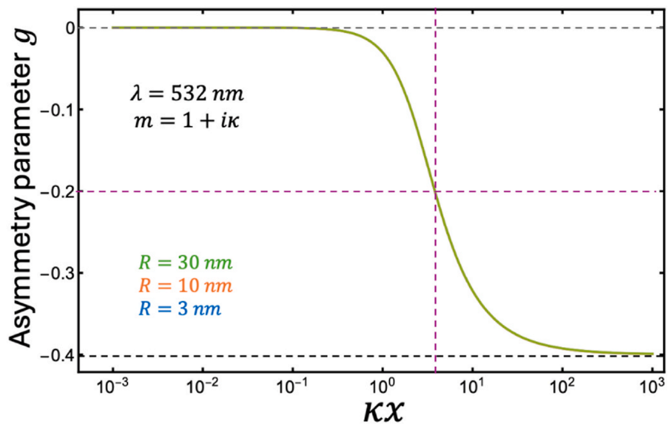

Fig. 3. | Asymmetry parameter g versus κx, as calculated using the Mie equations. κx was varied by holding R constant and changing κ. Three different values of R were plotted, and all three curves coincide. The black dashed line is the asymmetry parameter of SDA scattering, -0.4. The horizontal purple dashed line is half the SDA asymmetry parameter, -0.2.

using the series expansion of f about the origin. The series expansions for relevant functions are included in Bohren and Huffman. The first normal modes may be expressed as

$$a_1 \approx -i\frac{2x^3}{3}\frac{m\psi_1(mx) - \frac{1}{2}x\,\psi_1'(mx)}{m\psi_1(mx) + x\,\psi_1'(mx)}, \tag{7a}$$

$$b_1 \approx -i\frac{2x^3}{3}\frac{\psi_1(mx) - \frac{1}{2}mx\,\psi_1'(mx)}{\psi_1(mx) + mx\,\psi_1'(mx)}, \tag{7b}$$

$$a_2 = O(x^5), \tag{7c}$$

$$b_2 = O(x^5)\ . \tag{7d}$$

Here, $\psi_n(z)$ is the Ricatti-Bessel function of the first kind and $\psi_n'(z)$ is its derivative. Since we did not assume $|mx| \ll 1$, we did not expand terms of the form $f(mx)$. Under our assumption that $x \ll 1$, terms with $n > 1$ become negligible. For instance, for $x = 0.2$, the magnitudes of coefficients a_1 and b_1 are more than three orders of magnitude larger than a_2 and b_2, respectively for arbitrary κ. We therefore only retain terms with $n = 1$ for our analysis, where a_1 and b_1 correspond to the electric and magnetic dipole terms, respectively. Thus, small particle scattering may be represented simply as the sum of an electric and a magnetic dipole. Note that the case, where the condition $x \ll 1$ is satisfied but not the condition $|mx| \ll 1$, has been discussed previously in detail by Videen et al. [15] and García-Cámara et al. [16].

The angular dependence functions for $n = 1$ are given by

$$\pi_1(\cos\theta) = 1 \tag{8a}$$

$$\tau_1(\cos\theta) = \cos\theta\ . \tag{8b}$$

Next, we find it helpful to simplify a_1 and b_1 by writing them in terms of the following complex function

$$h(z) = \frac{z^2 \sin z}{\sin z - z\cos z}\ . \tag{9}$$

Noting that $\psi_1(z) = \frac{\sin z}{z} - \cos z$, we can express a_1 and b_1 as [13]

$$a_1 \approx -i\frac{2x^3}{3}\frac{m^2 + \frac{1}{2} - \frac{1}{2}h(mx)}{m^2 - 1 + h(mx)}, \tag{10a}$$

$$b_1 \approx -i\frac{2x^3}{3}\left(-\frac{h(mx) - 3}{2h(mx)}\right). \tag{10b}$$

Since $Re(mx) \ll 1$, mx is essentially an imaginary number with a small deviation in the real direction. (Note that we assumed $Re(mx) \ll 1$, which includes the case $m = 1 + i\kappa$. Our work therefore holds for arbitrary m as long as the real part isn't too large.) It can be shown that for imaginary z, $h(z)$ is stationary with respect to small deviations in the real component. Therefore, $h(mx) \approx h(i\kappa x)$. We define an auxiliary function $w : \mathbb{R} \to \mathbb{R}$ as follows

$$w(t) \equiv h(i\cdot t) = \frac{t^2 \sinh t}{t\cosh t - \sinh t}\ . \tag{11}$$

Now, $h(mx)$ may be replaced by $w(\kappa x)$. The simplifications made above will soon prove to be helpful when checking limiting cases, which can be visualized rather easily using Fig. (4) below. For small t, $w(t) \approx 3$, and for large t, $w(t) \approx t$. Incidentally, $w(t)$ nearly matches the hyperbolic function $\sqrt{t^2 + 9}$, with a maximum relative error of about 10%.

Moving on, we can determine the form of the angular dependence of the differential cross section. Keeping only the $n = 1$ terms in Eqs. (6a) and (6b), we obtain

$$\frac{dC_s}{d\Omega} \approx \frac{1}{k^2}\left|\frac{3}{2}(a_1 + b_1\cos\theta)\right|^2 \tag{12a}$$

$$\frac{dC_P}{d\Omega} \approx \frac{1}{k^2}\left|\frac{3}{2}(a_1\cos\theta + b_1)\right|^2\ . \tag{12b}$$

The reader may find it satisfying to see a formula for the differential cross section as a function of scale factor k^4R^6, refractive index m, scattering angle θ, and inverse relative optical penetration depth κx

$$\frac{dC_s}{d\Omega} = k^4R^6\left|\frac{m^2 + \frac{1}{2} - \frac{1}{2}w(\kappa x)}{m^2 - 1 + w(\kappa x)} - \frac{w(\kappa x) - 3}{2w(\kappa x)}\cos\theta\right|^2 \tag{13a}$$

$$\frac{dC_P}{d\Omega} = k^4R^6\left|\frac{m^2 + \frac{1}{2} - \frac{1}{2}w(\kappa x)}{m^2 - 1 + w(\kappa x)}\cos\theta - \frac{w(\kappa x) - 3}{2w(\kappa x)}\right|^2\ . \tag{13b}$$

The total scattering cross section is given by the following [13] as

$$C_{sca} = \frac{2\pi}{k^2}\sum_n (2n+1)\left(|a_n|^2 + |b_n|^2\right)$$
$$\approx \frac{8\pi k^4R^6}{3}\left(\left|\frac{m^2 + \frac{1}{2} - \frac{1}{2}w(\kappa x)}{m^2 - 1 + w(\kappa x)}\right|^2 + \left|\frac{w(\kappa x) - 3}{2w(\kappa x)}\right|^2\right)\ . \tag{14}$$

Now, our previously made simplifications become very helpful. With

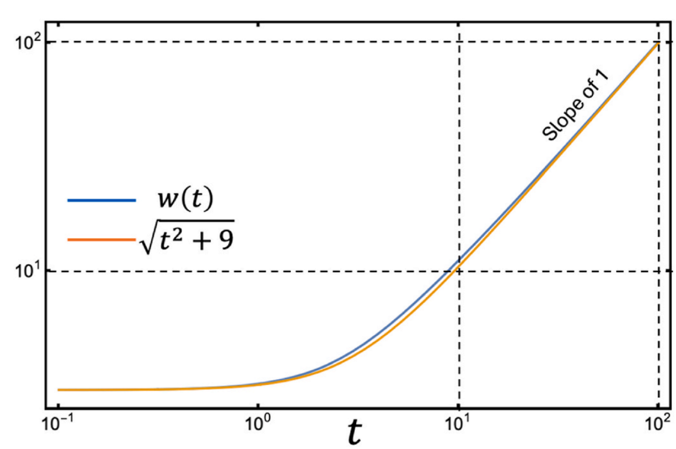

Fig. 4. | Log-log plot of the function w. w is plotted in blue, and the hyperbolic ansatz $\sqrt{t^2 + 9}$ is plotted in orange for comparison. The two functions are similar but show some slight disagreement between $t = 10^0$ and $t = 10^1$.

Eq. (13) and 14, we are no longer limited to the extreme cases of Rayleigh or SDA scattering. We now have a nearly turnkey formula for the scattering by $x \ll 1$ particles with $Re(mx) \ll 1$ and arbitrary κ—the only accessory needed is the function w.

One can painlessly check both the Rayleigh ($\kappa x \ll 1$) and the SDA ($\kappa x \gg 1$) limits of Eqs. (13) and (14). When $\kappa x \ll 1$, $w(\kappa x) \approx 3$, and we see that the magnetic dipole term vanishes while the electric dipole term reduces to the familiar Lorentz-Lorenz factor LL(m) seen in the ED formulation of Eq. (1). When $\kappa x \gg 1$, $w(\kappa x) \approx \kappa x$, and constants become negligible compared to $w(\kappa x)$. Note that $m^2 \gg w(\kappa x)$ in this situation since $x \ll 1$. Then, in the SDA limit, dependence on m washes out, and the ratio of the magnetic dipole term to the electric dipole term is $-1/2$, just as with SDA scattering.

Below, we plot this new equation and compare it to the Mie equations. But first, we do a rough estimate of error. Since a_1 and b_1 are proportional to x^3, the intensity is proportional to x^6. The next highest order correction to the intensity comes from cross terms between dipole and quadrupole moments, meaning it is on the order of $O(x^3 \cdot x^5) = O(x^8) = x^2 O(x^6)$, so the relative error is proportional to x^2.

In Fig. 5, we plot the scale-factor-normalized differential scattering cross section of s-polarized light using Eq. (13) and compare it to plots generated by the Mie equations.

For both particle sizes, the shapes of the curves are roughly conserved. When κx is small, the curves are flat; when κx gets large, the curves show enhanced backscattering and diminished forward scattering.

For the $x = 0.12$ particle (Fig. (5a)), both formulations agree very well, which makes sense since the relative error should be on the order of $x^2 \approx 1\%$. However, when the size parameter is increased to 0.35 (Fig. (5b)) , we notice quite a bit of disagreement, especially at $\kappa x = 1$. The maximum fractional difference between Mie and Eq. (13) in Fig. (5b) is around 15%, which is roughly in agreement with our error estimate of $x^2 \approx 10\%$. The quadrupole moment terms we neglected in deriving Eq. (13) are the root of most of the differences between Mie and Eq. (13) at this fringe value of the size parameter.

5. Visualization of the phenomenon

In this section, we qualitatively explain the cause of the asymmetry between forward and backward scattering using vectors. We show that

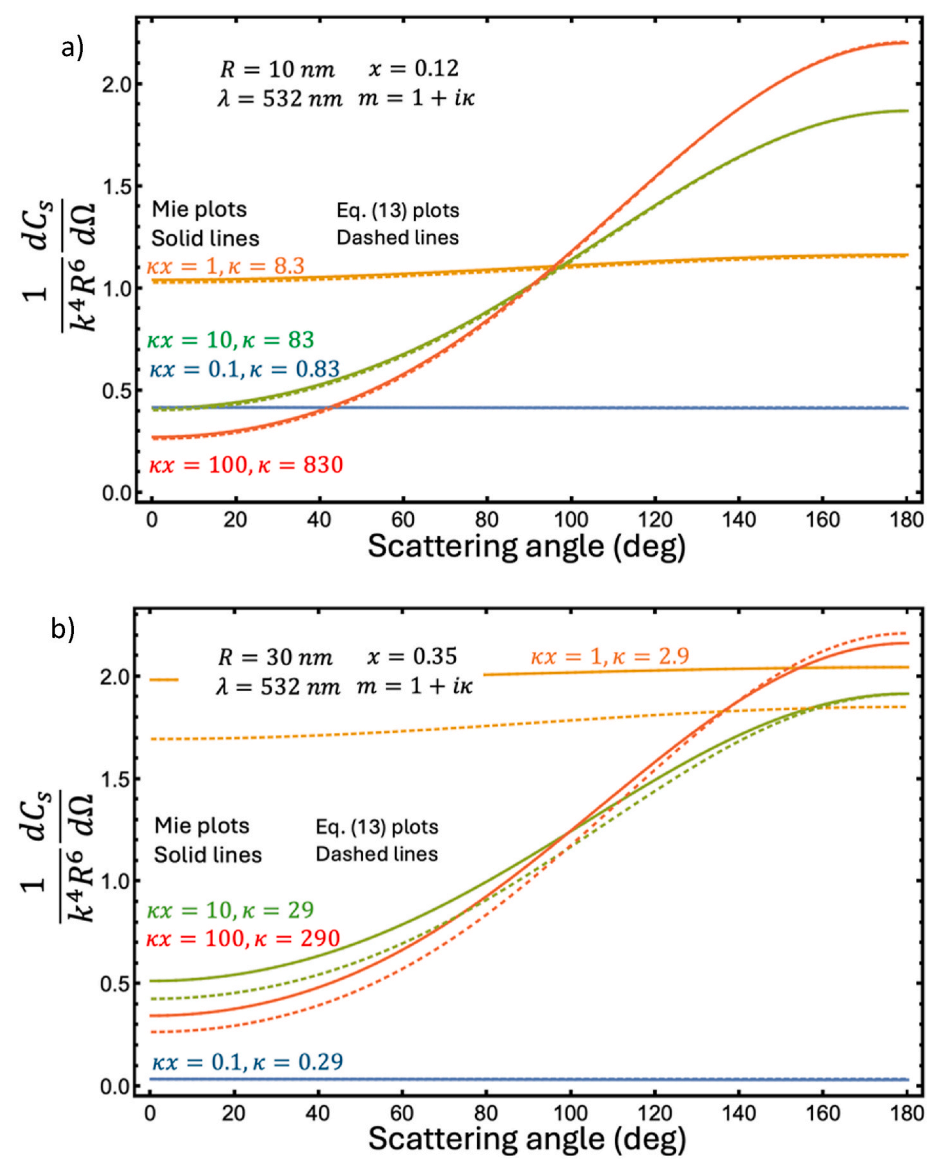

Fig. 5. | Differential scattering cross section of s-polarized light versus scattering angle for a spherical particle of radius (a) 10 nm and (b) 30 nm and incident light wavelength 532 nm. The solid plots were calculated using the Mie equations. The dashed lines were calculated using Eq. (13).

the reason for enhanced backscattering and damped forward scattering is constructive interference in the backward direction and destructive interference in the forward direction.

As in Fig. (6) below, take the $+x$-direction to be right, $+y$-direction upward, and $+z$-direction out of the plane of the page. We will consider s-polarized light. Let a plane wave of light of wavelength λ propagate in the $+x$-direction toward a spherical particle of radius $R \ll \lambda$. We consider a certain instant where the electric field of the incident wave near the particle is pointing in the $+z$-direction. Note that because of the constraint $R \ll \lambda$, the electric and magnetic fields are roughly uniform in the vicinity of the particle. Since $\hat{x} \times \hat{z} = \widehat{-y}$, the magnetic field of the incident wave points in the $-y$-direction.

Conduction with zero resistivity can be modeled by taking $\kappa \rightarrow \infty$ [4]. In the case of perfect conduction, boundary conditions require that the component of the electric field parallel to the surface of the conductor and the component of the magnetic field perpendicular to the surface of the conductor vanish [10]. We shall assume that in the case of finite κ, the particle will be an imperfect conductor, still "attempting" to satisfy these boundary conditions.

It may be shown that the electric field boundary condition can be satisfied by placing a point electric dipole at the center of the sphere with dipole moment pointing in the $+z$-direction, parallel to the incident electric field (note that the far field of an electric dipole points antiparallel to the dipole moment). Similarly, the magnetic field boundary condition can be satisfied by placing a point magnetic dipole at the center of the sphere with dipole moment pointing in the $+y$-direction, antiparallel to the incident magnetic field [10].

Let us consider the wave emitted by the electric dipole. In the forward direction, its electric field points in the $-z$-direction, antiparallel to the dipole moment, and the direction of propagation is the $+x$-direction; therefore, its magnetic field points in the $+y$-direction. In the backward direction, its electric field points in the $-z$-direction, and the direction of propagation is the $-x$-direction; therefore, its magnetic field points in the $-y$-direction.

Let us now consider the wave emitted by the magnetic dipole. In the forward direction, its magnetic field points in the $-y$-direction, antiparallel to the dipole moment, and the direction of propagation is the $+x$-direction; therefore, its electric field points in the $+z$-direction. In the backward direction, its magnetic field points in the $-y$-direction, antiparallel to the dipole moment, and the direction of propagation is the $-x$-direction; therefore, its electric field points in the $-z$-direction.

In the forward direction, the wave emitted by the electric dipole has an electric field pointing in the $-z$-direction, whereas the electric field from the magnetic dipole points in the $+z$-direction. So, in the forward direction, the two emitted waves interfere destructively, ultimately weakening the forward scattering intensity. By similar logic, in the backward direction, the waves interfere constructively, strengthening the scattering intensity in the backward direction. Note that even in the limit $\kappa \rightarrow \infty$, the field emitted by the magnetic dipole is weaker than that emitted by the electric dipole, so, for the s polarization, there is never a point at which the scattering intensity is zero.

6. Conclusions

We explored light scattering by a sphere of size parameter $x = \frac{2\pi R}{\lambda} \ll 1$ and a complex refractive index of the form $m = 1 + i\kappa$, where the real part was set to unity to represent submersion in a nonabsorbent medium of refractive index equal to the real component of the particle refractive index. In this case, scattering is caused by the imaginary part of the particle refractive index. We empirically find that the scattering follows Rayleigh scattering at small values of κ, transitioning to perfect conductor (SDA) scattering at large values of the imaginary part of the refractive index. As κ got larger, we found that the scattering becomes more and more biased to the backward direction, consistent with a negative asymmetry parameter. To explain our results theoretically, we turned to the Mie equations in the limit of small size parameters. Assuming the real part of the refractive index isn't too large, we found that the scattering can be described by a point electromagnetic dipole with electric and magnetic dipole moments determined by the Mie equations. We gave equations describing scattering by small particles with $Re(mx) \ll 1$ and arbitrary imaginary component of refractive index. These equations were plotted against the Mie equations to demonstrate their accuracy. Finally, a detailed explanation is given describing why backscattering was enhanced and forward scattering dimmed in the limit $\kappa \rightarrow \infty$. The scattering discussed in this paper may find application to situations with small scatterers whose real component of refractive index is matched to the medium refractive index—examples are the remote sensing of small phytoplankton and the determination of nanoparticle refractive index (by attempting to make the medium refractive index match the real part of the nanoparticle refractive index).

CRediT authorship contribution statement

Sami Labidi: Writing – review & editing, Writing – original draft,

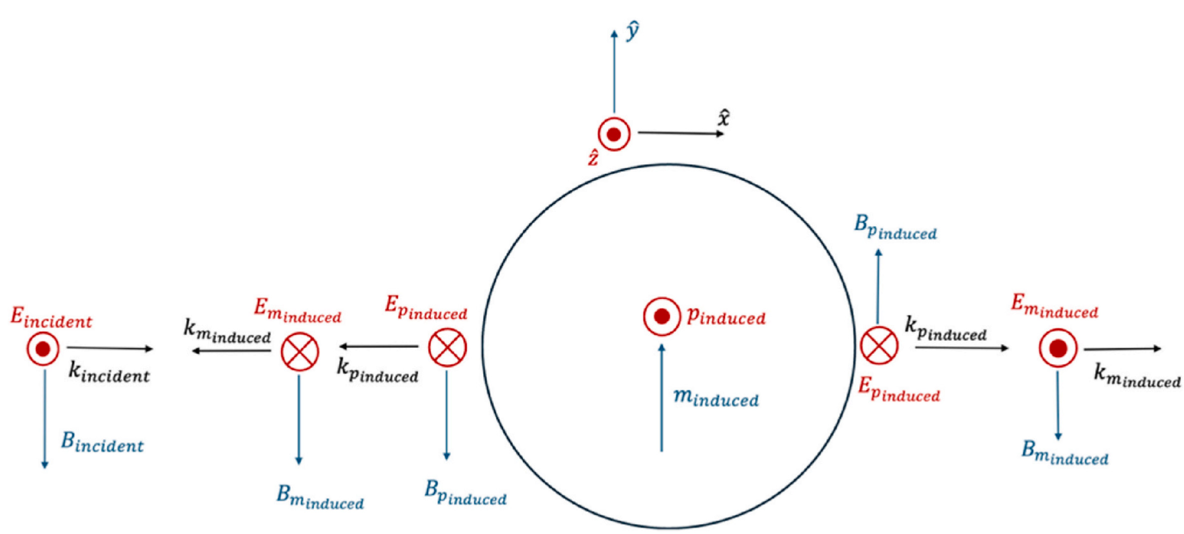

Fig. 6. | Diagram showing the incident wave, induced dipole moments, and emitted waves. The electric field, magnetic field, and wavevector are shown for all waves. Subscripts denote the source of the wave, if applicable; for example, $E_{p_{induced}}$ is the electric field emitted by $p_{induced}$, the induced electric dipole moment. In this diagram, m is the magnetic dipole moment and is not to be confused with the refractive index m.

Visualization, Methodology, Investigation, Formal analysis. **Justin B. Maughan:** Writing – review & editing, Writing – original draft, Visualization, Methodology, Investigation, Formal analysis. **Kurt Ehlers:** Writing – review & editing, Writing – original draft, Visualization, Methodology, Investigation, Formal analysis. **Prakash Gautam:** Writing – review & editing, Investigation. **Christopher M. Sorensen:** Writing – review & editing, Methodology, Investigation, Funding acquisition. **Hans Moosmüller:** Writing – review & editing, Writing – original draft, Methodology, Investigation, Funding acquisition, Formal analysis, Conceptualization.

Funding

This work was supported in part by the Department of Energy (DOE) Los Alamos National Laboratory (LANL) through Kansas State University (KSU) under Grant No. A23-0465-S001 and by the National Science Foundation under grant No. AGM 1649783 and No. OIA-2148788.

Declaration of competing interest

The authors declare that they have no known competing financial interests or personal relationships that could have appeared to influence the work reported in this paper.

Data availability

No data was used for the research described in the article.

References

[1] K. Ehlers, H. Moosmüller, Small and large particle limits of the asymmetry parameter for homogeneous, spherical particles, Aerosol. Sci. Technol. 57 (2023) 425–433.
[2] C.M. Sorensen, Light Scattering and Absorption by Particles, IOP Publishing, 2022.
[3] E.J. Meehan, J.K. Miller, Complex refractive index of colloidal silver bromide in the near-ultraviolet, J Phys Chem 72 (1968) 1523–1529.
[4] H.C. van de Hulst, Light Scattering by Small Particles, Dover Publications, New York, 1981.
[5] R.E. Green, H.M. Sosik, R.J. Olson, M.D. DuRand, Flow cytometric determination of size and complex refractive index for marine particles: comparison with independent and bulk estimates, Appl. Opt. 42 (2003) 526–541.
[6] H. Moosmüller, J.B. Maughan, P. Gautam, C.M. Sorensen, A mixing rule for imaginary parts of refractive indices of aerosols or colloids in the Rayleigh regime, J. Quant. Spectrosc. Radiat. Transfer 331 (2025) 109254.
[7] J.B. Maughan, H. Moosmüller, P. Gautam, C.M. Sorensen, Retrieval of Complex Refractive Index Spectra Using Colloids in the Rayleigh Regime: Theory, J Quant Spectrosc Radiat Transfer, 2025 in preparation.
[8] J.B. Maughan, C.M. Sorensen, Universal parameter to describe the reduction of refraction effects in the scattering of absorbing spheres, J Opt Soc Am A 37 (2020) 1456–1464.
[9] C.M. Sorensen, J.B. Maughan, H. Moosmüller, Spherical particle absorption over a broad range of imaginary refractive index, J. Quant. Spectrosc. Radiat. Transfer 226 (2019) 81–86.
[10] J.D. Jackson, Classical Electrodynamics, John Wiley & Sons, 2021.
[11] H.A. Lorentz, Ueber die Beziehung zwischen der Fortpflanzungsgeschwindigkeit des Lichtes und der Körperdichte, Ann Phys 245 (1880) 641–665.
[12] L. Lorenz, Ueber die Refractionsconstante, Ann Phys 247 (1880) 70–103.
[13] C.F. Bohren, D.R. Huffman, Absorption and Scattering of Light by Small Particles, Wiley, New York, 1998.
[14] H. Moosmüller, C.M. Sorensen, Small and large particle limits of single scattering albedo for homogeneous, spherical particles, J. Quant. Spectrosc. Radiat. Transf. 204 (2018) 250–255.
[15] G. Videen, W.S. Bickel, Light-scattering resonances in small spheres, Phys. Rev. 45 (1992) 6008–6012.
[16] B. García-Cámara, F. Moreno, F. González, J.M. Saiz, G. Videen, Light scattering resonances in small particles with electric and magnetic properties, J Opt Soc Am A 25 (2008) 327–334.